PNWD-3126

Hydrologic Response to Landscape Structures at H.J. Andrews Experimental Forest

Scott R. Waichler

Pacific Northwest National Laboratory
MSIN K9-36, P.O. Box 999
Richland, Washington, 99352
scott.waichler@pnl.gov

December 2001

Prepared for Dr. Steve Garman, Oregon State University
Battelle Agreement 42725, OSU Purchase Order P0048640

LEGAL NOTICE

This document was printed on recycled paper.
(9/97)

Summary

The Distributed Hydrology-Soil-Vegetation Model (DHSVM) was used to evaluate hydrologic impacts of hypothetical landscape structures in H.J. Andrews Experimental Forest Watershed 1. Landscape structures were defined by patterns of oldgrowth and clearcut areas, where vegetation properties of each land cover type were constant in time. Twenty different landscape structures were defined with various levels of total clearcut area, patch size, and patch distributions. DHSVM was run over water years 1980-98 for each landscape structure, and the predicted mean annual streamflow, mean annual evapotranspiration, and daily streamflow responses were compared across landscape structures. Overall, hydrologic response was primarily and linearly related to total clearcut area. Some minor nonlinearity was evident in the daily streamflow and mean annual fluxes. Distribution type for small patch size was not significant, but locating large patchcuts in the riparian zone did result in more streamflow at moderate flow levels compared to locating large patchcuts in the top or bottom of the watershed.

Contents

Figures

Introduction

The impacts of forest practices on catchment hydrology are an important problem in resource management and science. One aspect of the problem is how water fluxes depend on size and distribution of clearcut patches within a catchment. Do fluxes change linearly with respect to total clearcut area, or non-linearly? Do hydrologic impacts depend on the type of patch distribution, for example random vs. even? The purpose of this study, prepared for Dr. Steve Garman/Oregon State University, is to answer these questions by applying the Distributed Hydrology-Soil-Vegetation Model (DHSVM) to 20 landscape structures (scenarios) in watershed 1 (WS1) of the H.J. Andrews Experimental Forest (HJA) (Figure 1). The HJA dataset includes long-term climate and streamflow records that have been used in many studies of watershed response to forest harvesting. The dataset has been relatively little used to support modeling of watershed processes, however. Modeling as a research method is an excellent way to generate hypotheses and preliminary answers where field experiments are impossible, such as the multiple land cover configurations studied here.

DHSVM is a physically-based model with fully explicit spatial representation of the landscape, at the resolution of available digital topography. DHSVM was calibrated on WS1 streamflow data from the WY58-62 period when the vegetation cover was oldgrowth Douglas fir/Western hemlock forest. Landscape structures consisting of various size clearcut patches and distributions of those patches were devised by Dr. Garman. DHSVM was then applied to the time period of best meteorological data, WY80-98, using the 20 landscape structures as maps of vegetation type. The predicted streamflow and evapotranspiration (ET) from these model runs indicated that hydrologic differences were primarily related to total clearcut area, and that the relationship was essentially linear.

Model Description

The Distributed Hydrology Soil Vegetation Model (DHSVM) is a process-based, distributed parameter hydrologic model that allows the simulation of runoff processes in forested, mountainous environments (Wigmosta et al., 1994). Recent applications of the model have evaluated the impacts of forest harvesting and road construction on watersheds in western Washington (LaMarche and Lettenmeier, 2001) and western British Columbia (Wigmosta and Perkins, 1997). A particular strength of DHSVM is its grid-based representation of the watershed, allowing specification of vegetation and soil types at the resolution of the digital elevation model (DEM). Elevation data of the DEM are used to simulate topographic controls on absorbed shortwave radiation, precipitation, air temperature and downslope water movement

Major processes simulated are canopy interception, evaporation, transpiration, snow accumulation and melt in the canopy and on the ground, vertical unsaturated water flow, and lateral saturated groundwater flow. The major inputs are grids of surface elevation, soil type, soil thickness, vegetation type; look-up tables of soil and vegetation biophysical parameter values; and timeseries of the climate variables air temperature, precipitation, wind speed, relative humidity, solar radiation, and longwave radiation from one or more stations. In the version used here, local climate data are mapped to each cell during the model run using lapse rates for vertical distribution of temperature and precipitation. Incoming solar radiation is adjusted according to topographic slope and aspect. Canopy evapotranspiration is simulated for each cell with the Penman-Monteith equation and local aerodynamic and canopy resistances. An explicit energy-balance approach is used for snow accumulation and ablation, both in the canopy and on the ground. Unsaturated soil water movement is downward only and driven by a unit gradient with hydraulic conductivity as a function of soil moisture content, using the Brooks-Corey equation. Lateral saturated soil water movement is simulated with Darcy's Law, where hydraulic gradient is based on either land surface or water table elevations (land surface option was used here).

Surface overland flow is generated where the water table rises above the land surface. Quick flow (i.e. macropore flow) is an important mechanism for streamflow generation in steep, temperate forests, and is represented by limiting infiltration into the soil matrix using the Holtan equation (Holtan, 1961) and directing more water into surface runoff than would otherwise be indicated by forest soil with high infiltration capacity. The surface runoff is then routed using a simple kinematic approach or a hydraulic approach of (Szilagyi and Parlange, 1999); the kinematic method was used here. Streamflow is generated by channel interception of surface and subsurface runoff. Vegetation may be represented with up to two layers. An overstory, if present, may cover all or some fraction of the cell. An understory, if present, is assumed to cover the entire cell. Vegetation types ranging from bare soil to low-lying vegetation to closed-canopy forests with understory may be specified. Climate variables are specified at a height above the top of the vegetation. Wind speed and solar radiation are attenuated down through the vegetation layers based on fractional area covered, vegetation height, and LAI. Stomatal resistance is computed separately for each root zone-vegetation layer combination, using soil moisture (Feddes et al., 1978), and air temperature, vapor pressure deficit, solar radiation (Dickinson et al., 1991).

Model Application

A regional 10-meter DEM and the WS1 gaging station location were obtained from the HJA databank and used to define WS1. Standard ArcInfo algorithms (ESRI, 1999) were used to process the DEM to fill erroneous sinks, calculate flow direction and flow accumulation, and delineate the watershed (Figure 1). The stream channel network was defined using a minimum contributing area of 35 cells (0.35 ha).

A soil type map in vector format was obtained from the HJA databank and converted to a 10-meter grid cell format using the ArcInfo polygrid function. Soils were characterized as having three rooting zones and a bottom zone. Soil depth and other properties for the seven soil types found in WS1 were compiled from Dyrness (1969) and Bredensteiner (1998). Additional soil parameters were calculated using methods found in Cosby et al. (1984) and Clapp and Hornberger (1978)

Vegetation in WS1 was represented as two types, oldgrowth and clearcut, in varying proportions and distributions in the 20 landscape scenarios. The oldgrowth type was defined as having an overstory leaf area index (LAI) of 8.5, and a height of 60 m. The oldgrowth understory was defined with LAI=0.5 and height=1 m. The same understory but no overstory were specified for the clearcut vegetation type.

Four types of clearcut patch distribution were defined by Dr. Garman: 1) Miscellaneous topographic distributions; 2) Random distribution with a minimum patch size of 1 cell; 3) Random distribution with a minimum patch size of 9x9 cells; 4) Even distribution with a minimum patch size of 3x3 cells (Figures 2- 5). For the Miscellaneous topographic distributions, three schemes were defined in addition to 0% clearcut (oldgrowth) and 100% clearcut: 1) 25% clearcut with patches located in upper portion of watershed; 2) 25% clearcut with patches in lower portion; and 3) 25% clearcut with patches located in the riparian zone. In the other distribution types (2-4), five levels of total area cut were defined: 5%, 10%, 25%, 50%, 75%.

Climate input to the model was obtained from the PRIMET and CS2MET stations, located 1-2km from the WS1. For the calibration period of WY58-62, hourly climate data were generated from daily minimum and maximum air temperature and relative humidity, and precipitation from CS2MET. For the main simulations involving WY80-98, hourly air temperature, precipitation, relative humidity, wind speed, and solar radiation from PRIMET were used, plus derived longwave radiation.

The model was calibrated using climate and streamflow data from the pre-harvest years of WY58-62, and a 100% oldgrowth vegetation cover. The primary parameters that were calibrated were lateral hydraulic conductivity, and the ratio of lateral to vertical hydraulic conductivity in the upper soil layer, which governs the amount of water entering quickflow and regular matrix flow. Model skill in simulating hourly streamflow was good; for WY58-62, R-squared=0.807, E=0.787, E1'=0.480, d1'=0.746, and bias=0.986 (see Appendix for explanation of statistical measures).

Results

Overall, the predicted hydrologic response to the amount of clearcut area is linear and similar for different distribution types. Mean annual runoff increases with total clearcut area (Figure 6), and mean annual ET decreases with clearcut area (Figure 7). A small amount of nonlinearity is indicated in Figures 6a,c. At each level of clearcut area, fluxes are similar across distribution types.

Daily streamflows were also evaluated. Hourly streamflow was aggregated to a daily timestep and then the upper 50 percent of daily flows were selected for further analysis. The percent change in streamflow from the oldgrowth state to the treated state, relative to the oldgrowth state, was plotted against streamflow probability (Figures 8,9). All three distribution types with clearcut area ranging from 5 to 75 percent exhibit some nonlinearity in the streamflow changes–at flows near the median, the increase between the 25% and 50% clearcut levels is slightly larger than the increases between other clearcut levels separated by 25% (Figure 8). For flows in the upper decile, the largest increase is between the 50% and 75% levels (Figure 9). For the miscellaneous topographic distributions involving large patches, the riparian scheme resulted in higher streamflow near the streamflow median than the other 25% clearcut distributions (Figure 8d). This is attributable to the absence of strong transpiration in an area where soil moisture is not limiting, resulting in more streamflow under the harvest scenario at times of moderate precipitation, snowmelt, and runoff.

To look more closely at peakflows, maximum hourly flow for each year (annual maximum series) was plotted for each landscape structure (Figure 10). For these highest flows, there was little difference between structures, reflecting the low buffering capacity of vegetation cover during high-intensity storms.

Discussion

Vegetation properties remained constant in time, so differences in hydrologic response between oldgrowth and clearcut areas also remained constant. In reality, regrowth would occur in the clearcut areas, resulting in decreasing hydrologic differences through time.

Mean annual fluxes depended primarily upon the total clearcut area, and the relationship was mostly linear. There was some evidence of nonlinear response in daily streamflows. The influence of topographic distribution of large patches was minor. Based on the results for streamflow and evapotranspiration, nonlinear hydrologic response was not an important outcome from this experiment.

Variation in hydrologic state variables (e.g. soil moisture) and flux variables (e.g., transpiration) in DHSVM is driven primarily by topographic position. Here, elevation was used to vary temperature; slope and aspect were used to vary incident solar radiation. Variability in solar radiation affects evapotranspiration and snowmelt. Other climate inputs (precipitation, relative humidity, wind speed) were assumed to be uniform across the watershed. The downslope movement of water drives variation in soil moisture, which affects transpiration and streamflow generation. The model can be expected to be sensitive to spatial pattern in vegetation when the mean climate or mean hillslope position of the vegetation types varies. In this experiment, the topographic extent and climatic range of the watershed were small, and vegetation types were distributed across all hillslope positions, except in the case of large riparian patches. Greater hydrologic response to spatial pattern of vegetation would be expected in a simulation where the climatic range within the watershed is greater, and where the vegetation distributions coincide to a greater degree with the climatic variability. Greater hydrologic response would also be expected where vegetation distribution depends strongly on hillslope position. Little difference was seen between the upper and lower 25% patchcut distributions because both involved patch placement along the hillslope from stream channel to ridgetop, and had similar average solar radiation inputs and air temperatures. Greater variation in climate and concentration of patches in distinct hillslope and climatic zones would cause greater differences in the mean hydrologic response of the watershed scenarios.

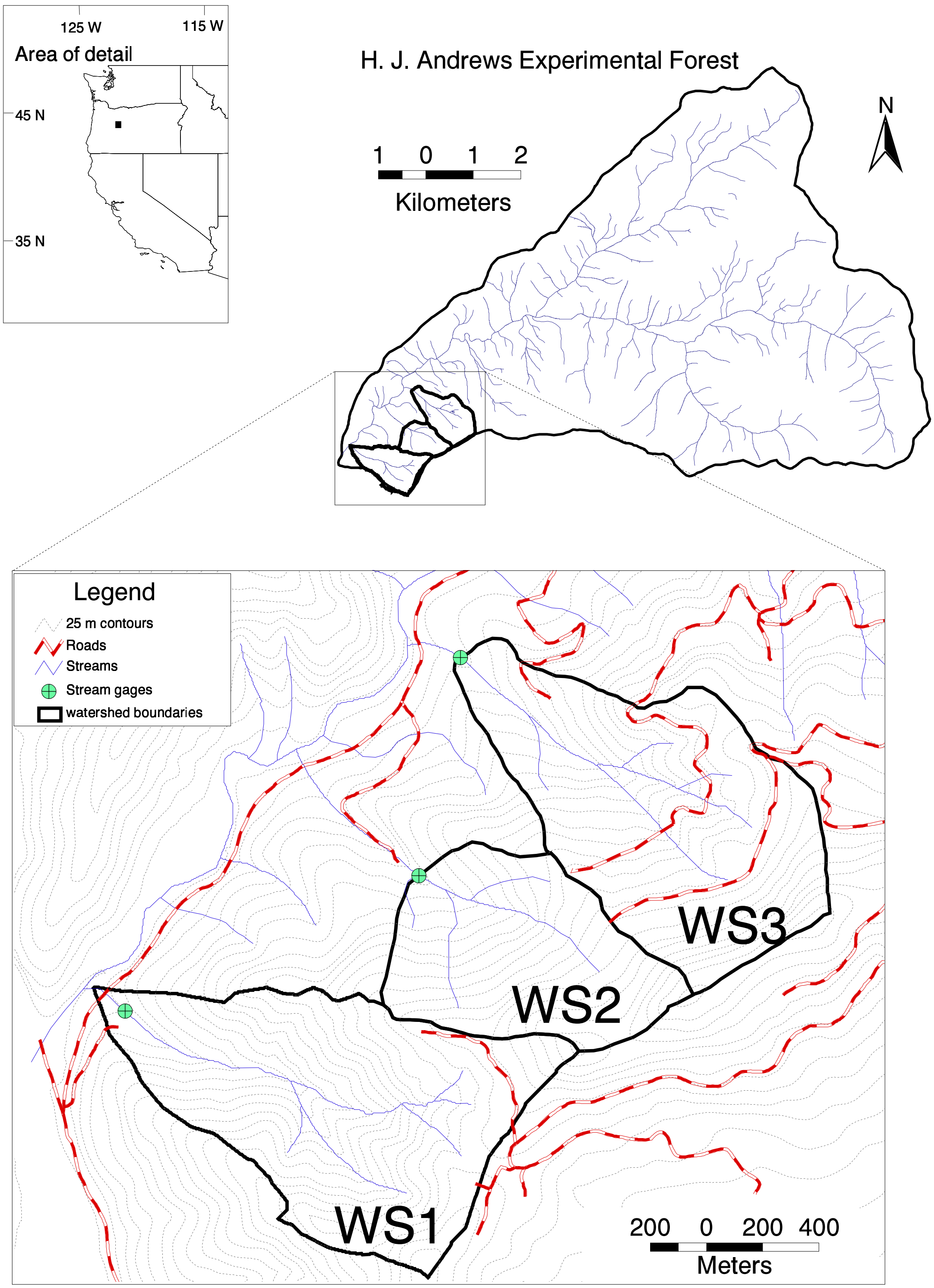

Figure 1: H.J. Andrews Experimental Forest and WS1. Graphic provided by Beverly Wemple, University of Vermont.

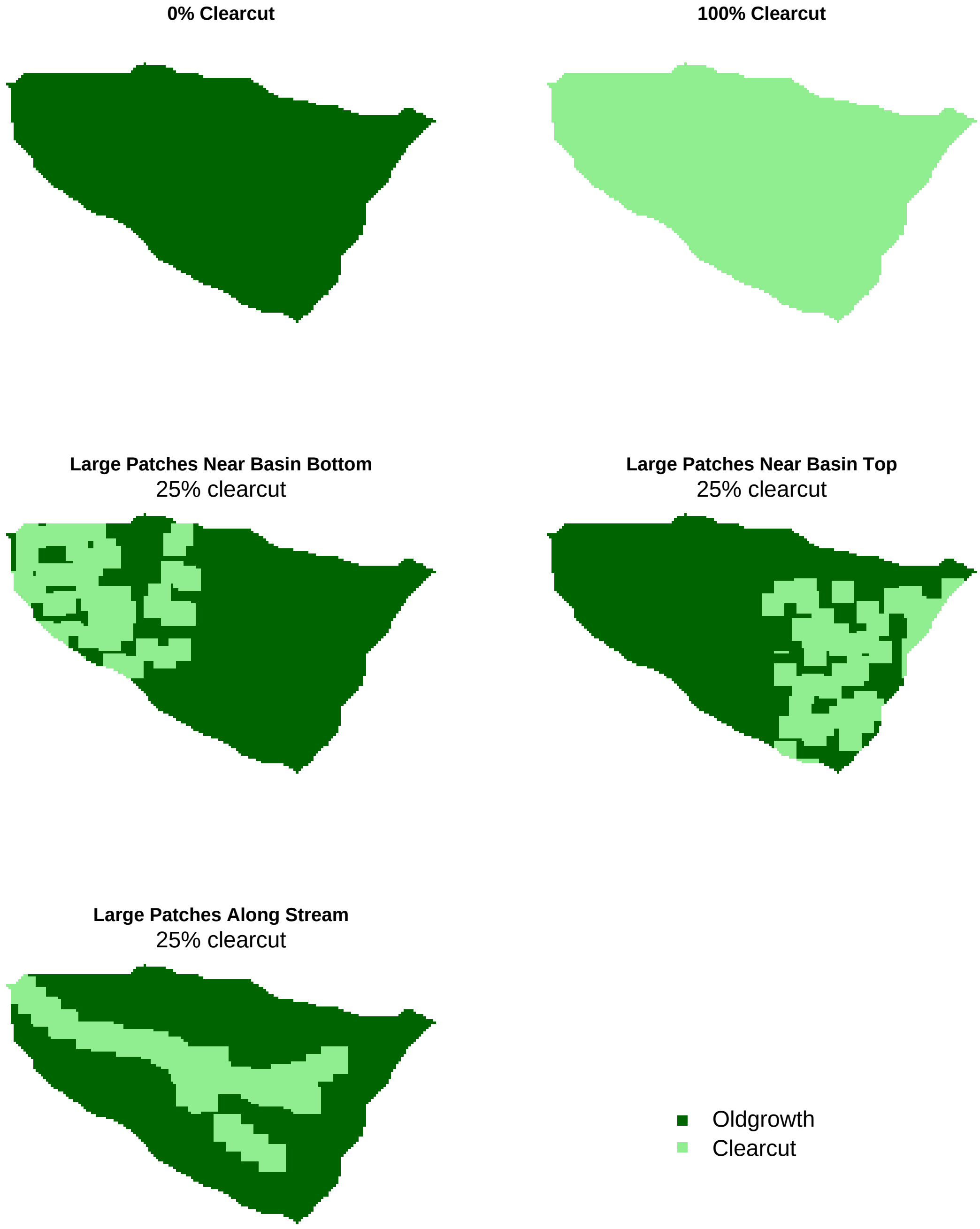

Figure 2: Miscellaneous clearcut distribution types.

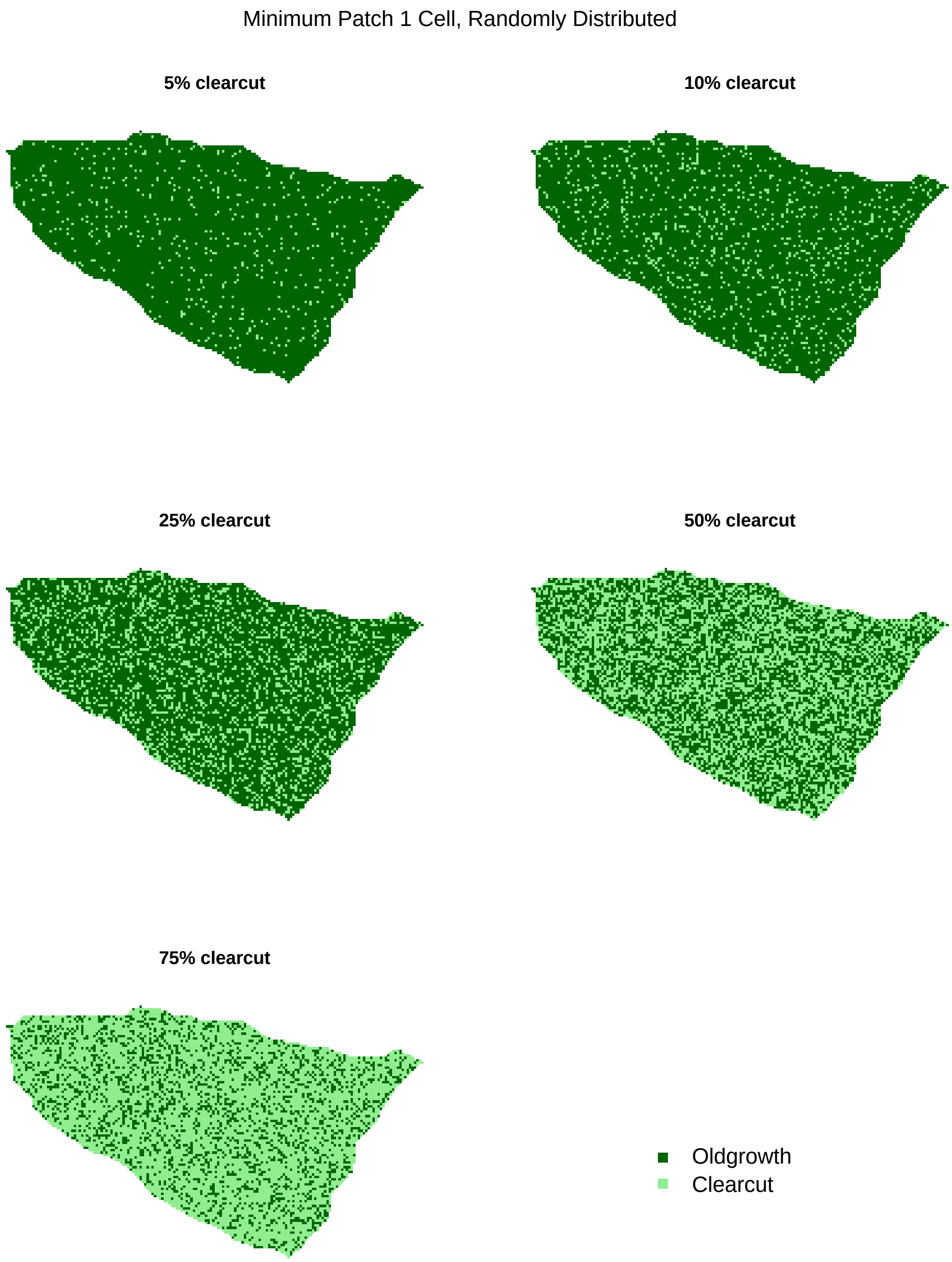

Figure 3: Randomly distributed clearcuts, with minimum patch size = 1 cell.

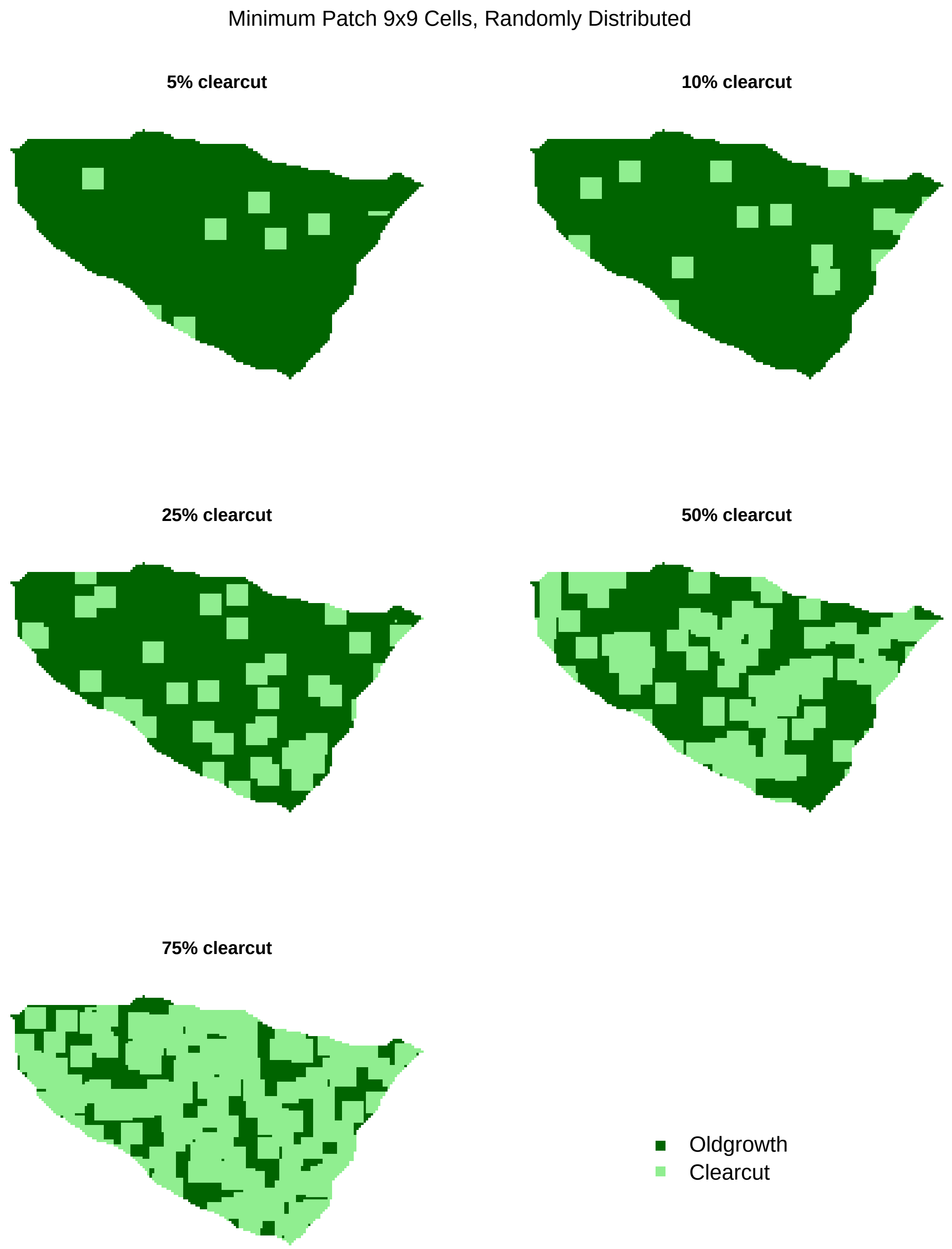

Figure 4: Randomly distributed clearcuts, with minimum patch size = 9x9 cells.

Figure 5: Evenly distributed clearcuts, with minimum patch size = 3x3 cells.

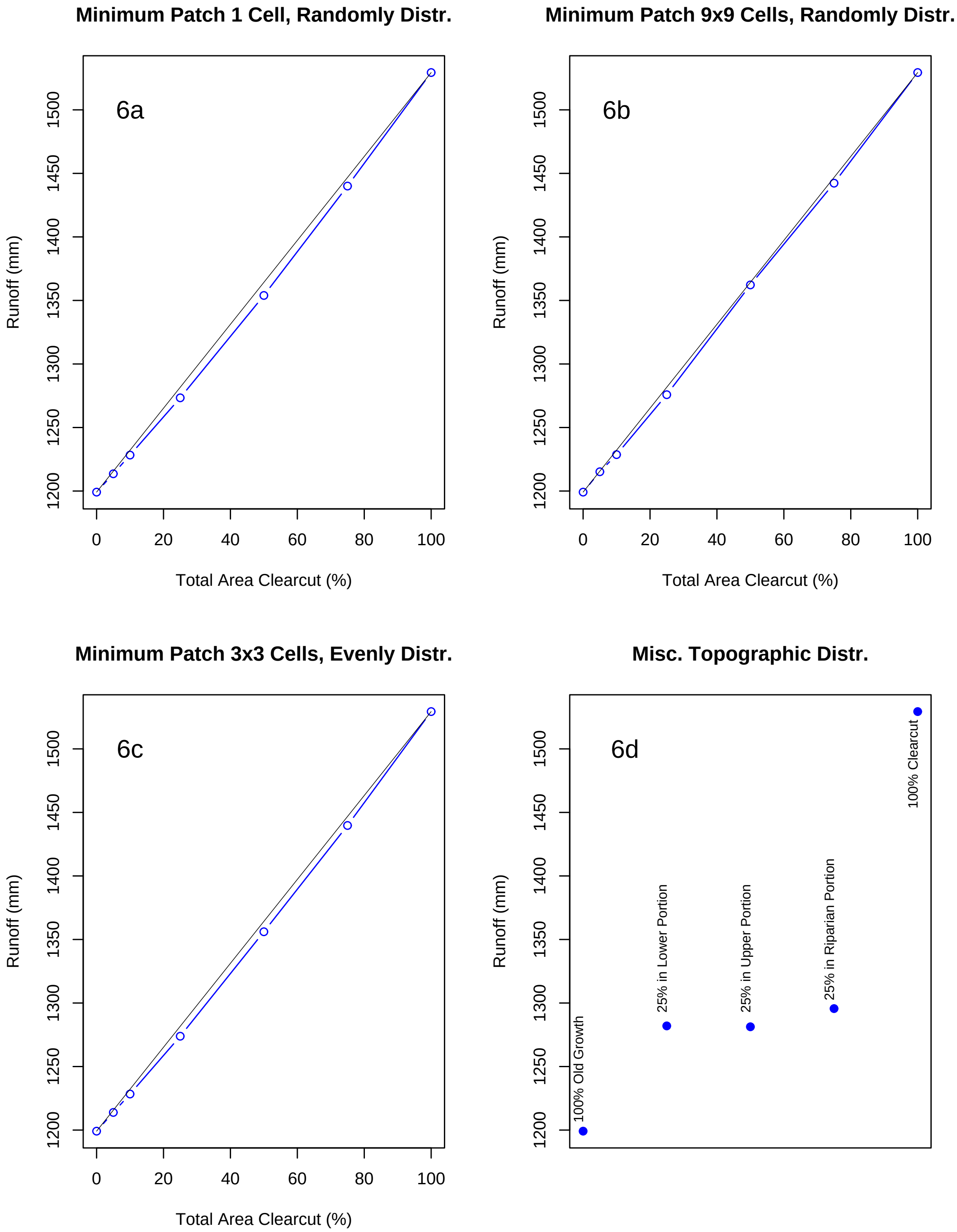

Figure 6: Mean annual runoff (streamflow), WY80-98, for different distribution types and levels of clearcut area. Thin black line is straight line segment between oldgrowth and 100% clearcut states.

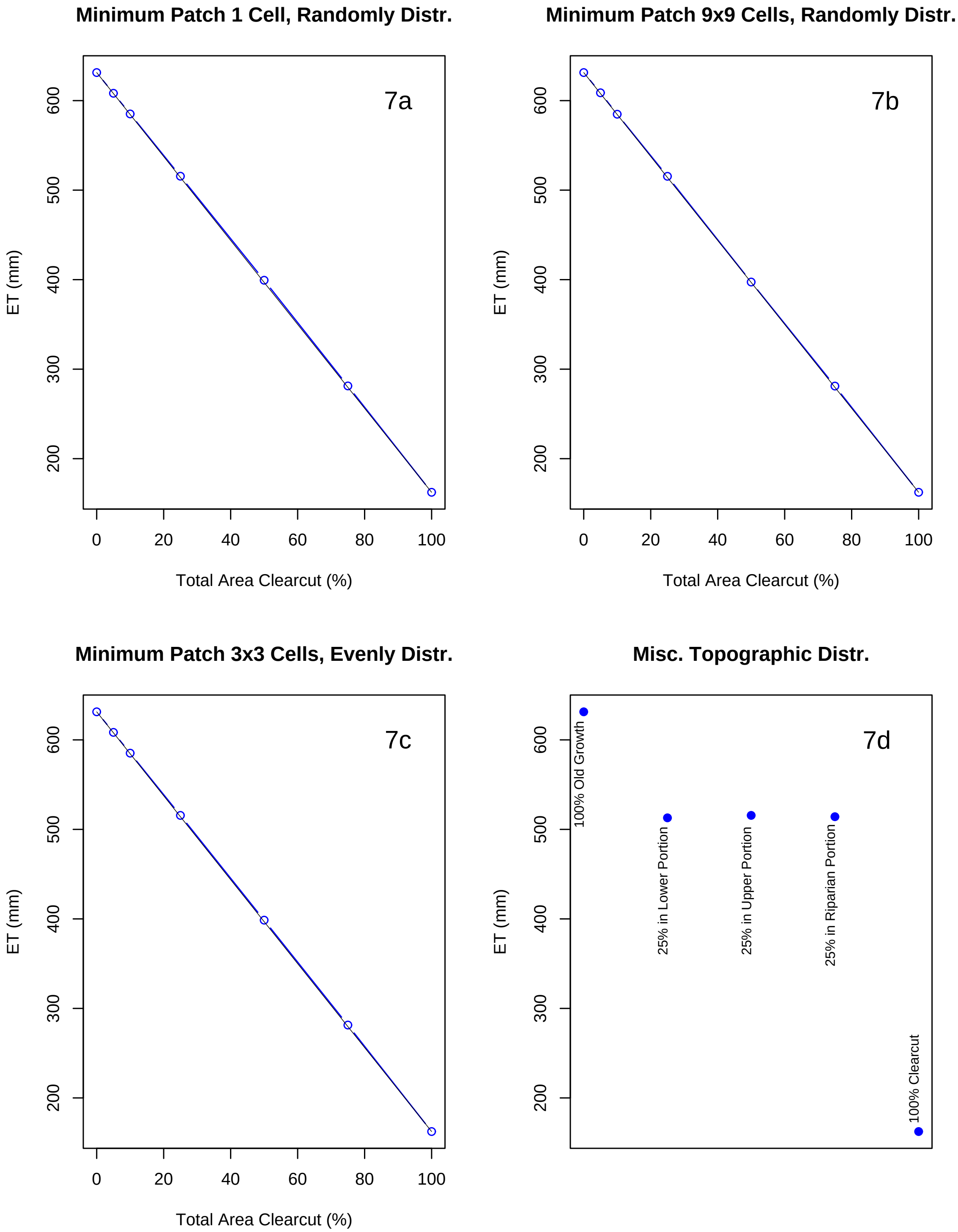

Figure 7: Mean annual evapotranspiration, WY80-98, for different distribution types and levels of clearcut area. Thin black line is straight line segment between oldgrowth and 100% clearcut states.

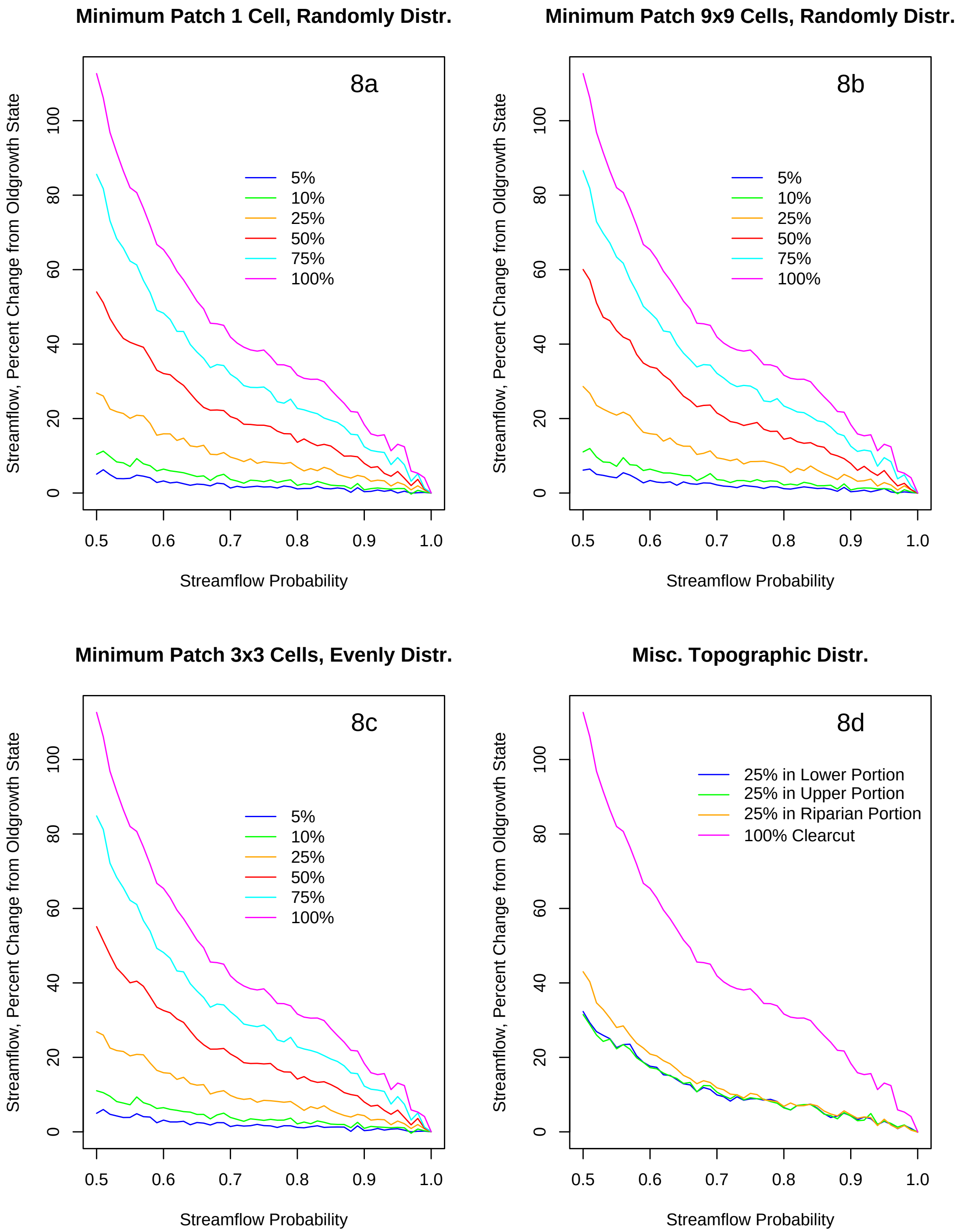

Figure 8: Percent change in daily streamflow (runoff) between treated state and oldgrowth state, relative to oldgrowth state, at streamflow probabilities ranging from the median (0.5) to maximum flow (1.0). Streamflow probability = cumulative density function, the probability of a flow being less than or equal to the given streamflow.

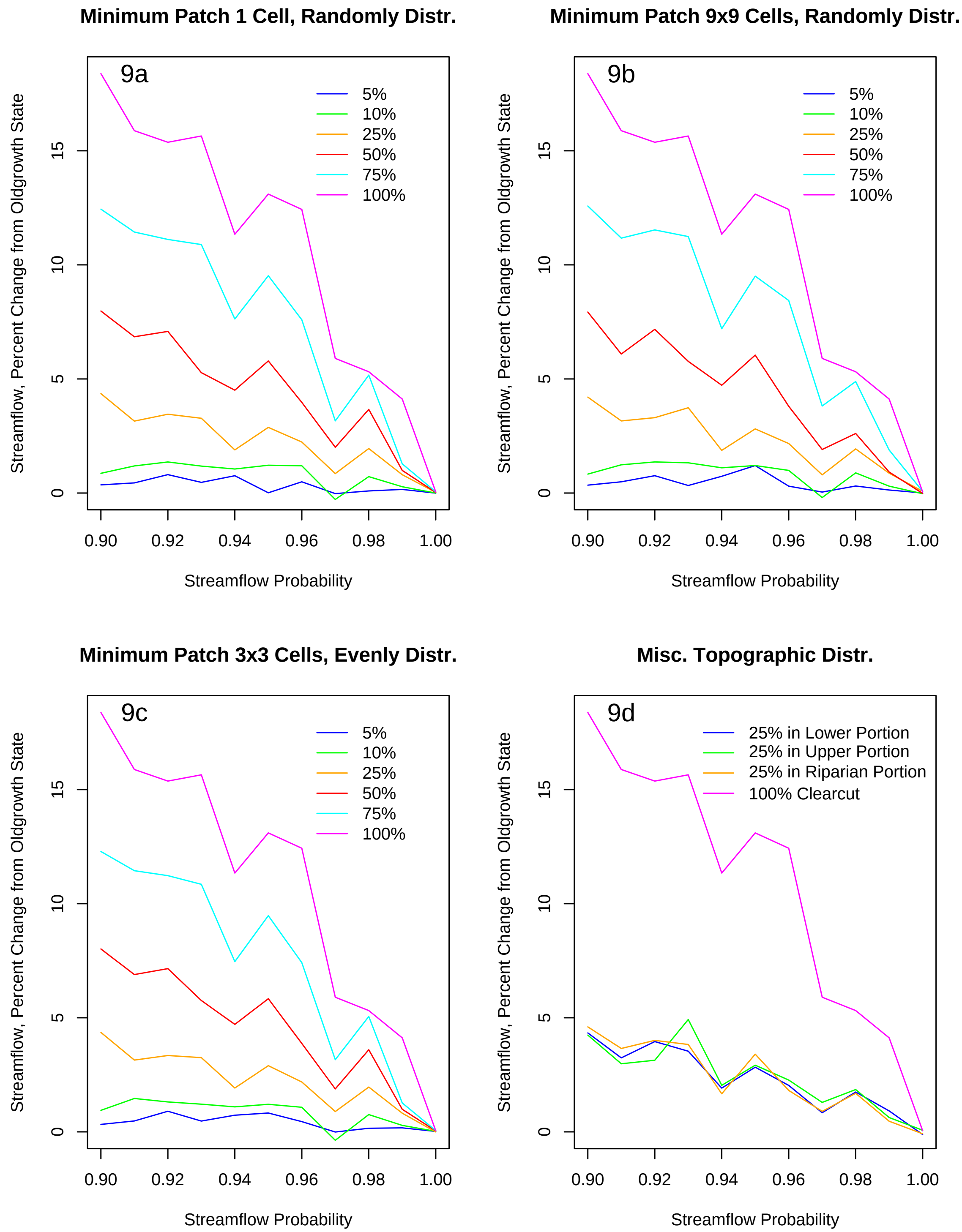

Figure 9: Percent change in daily streamflow (runoff) between treated state and oldgrowth state, relative to oldgrowth state, at streamflow probabilities ranging from 0.9 to 1.0. Streamflow probability = cumulative density function, the probability of a flow being less than or equal to the given streamflow.

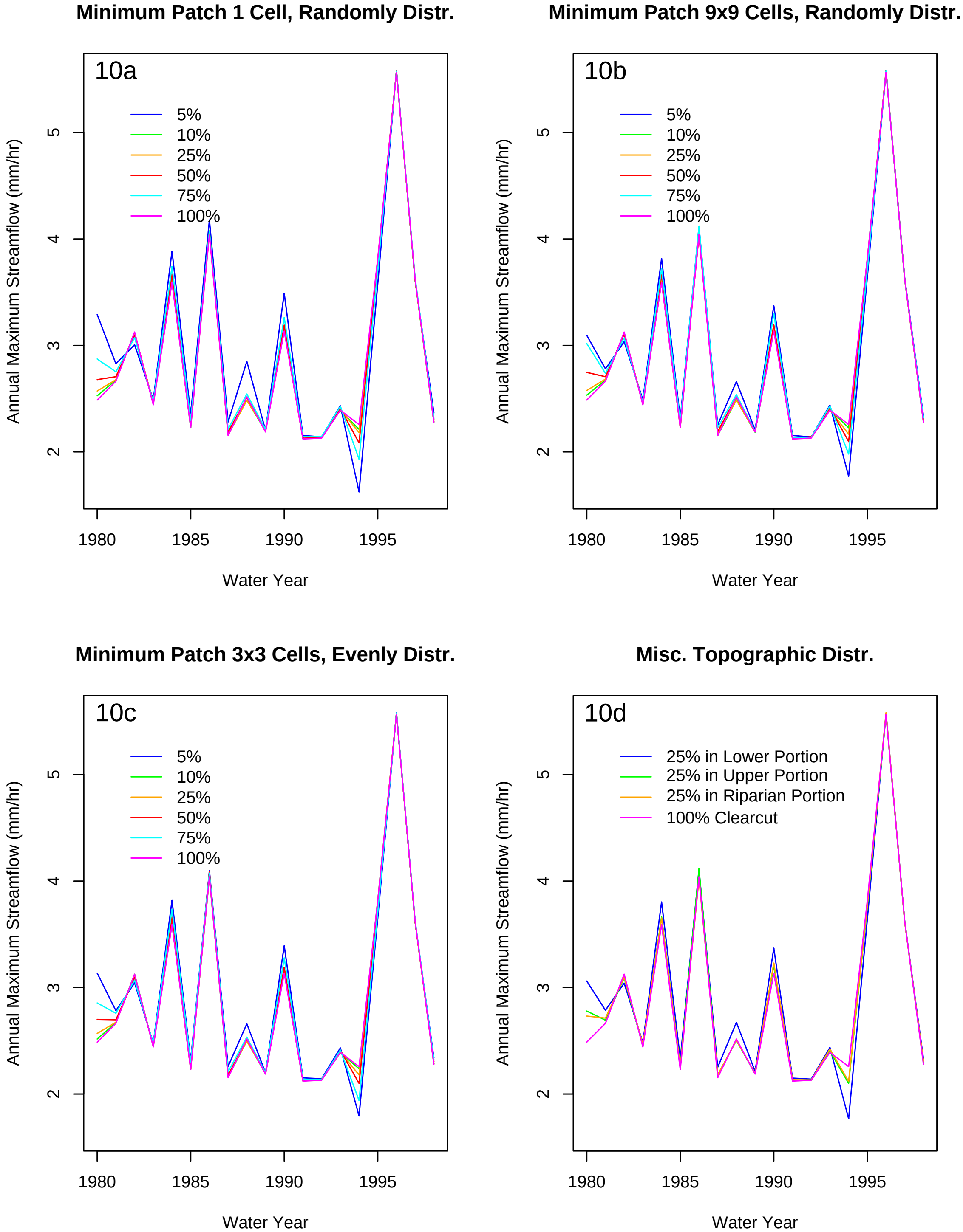

Figure 10: Annual maximum streamflows in mm/hr. Time basis in water years, October 1 to September 30.

References

Bredensteiner, K. C. (1998). An Investigation of Vegetation-Hydrology Interactions in Watershed 1 at the H. J. Andrews Experimental Forest. Master's thesis, Oregon State University, Corvallis, OR. 168 pp.

Clapp, R. and Hornberger, G. (1978). Empirical Equations for Some Soil Hydraulic Properties. *Water Resources Research*, 14(4):601–604.

Cosby, B., Hornberger, G., Clapp, R., and Ginn, T. (1984). A statistical exploration of the relationships of soil moisture characteristics to the physical properties of soils. *Water Resources Research*, 20(6):682–690.

Dickinson, R., Henderson-Sellers, A., Rosenzweig, C., and Sellers, P. (1991). Evapotranspiration models with canopy resistance for use in climate models, a review. *Agricultural and Forest Meteorology*, 54:373–388.

Dyrness, C. (1969). Hydrologic properties of soils on three small watersheds in the western Cascades of Oregon. Technical report, Forest and Range Experiment Station, USDA, Portland, OR. Pacific Northwest Research Note.

ESRI (1999). *ArcInfo version 8.0.1 and ArcDoc 8.0.1 on-line documentation*. Redlands, CA.

Feddes, R., Kowalik, P., and Zaradny, H. (1978). *Simulation of field water use and crop yield*. Wiley, New York. 188 pp.

Holtan, H. (1961). A concept of infiltration estimates in watershed engineering. Technical report, USDA, Washington, D.C. Paper 41-51.

LaMarche, J. L. and Lettenmeier, D. P. (2001). Effects of forest roads on flood flows in the Deschutes River, Washington. *Earth Surface Processes and Landforms*, 26:115–134.

Legates, D. and McCabe, G. (1999). Evaluating the use of 'goodness-of-fit' measures in hydrologic and hydroclimatic model validation. *Water Resources Research*, 35(1):233–241.

Nash, J. and Sutcliffe, J. (1970). River flow forecasting through conceptual models, Part 1 - A discussion of principles. *Journal of Hydrology*, 10:282–290.

Szilagyi, J. and Parlange, M. B. (1999). A geomorphology-based semi-distributed watershed model. *Advances in Water Resources*, 23:177–187.

Wigmosta, M. S., Vail, L. W., and Lettenmaier, D. P. (1994). A distributed hydrology-vegetation model for complex terrain. *Water Resources Research*, 30(6):1665–1679.

Wigmosta, M. W. and Perkins, W. P. (1997). A GIS-based modeling system for watershed analysis. Technical report, National Council of the Paper Industry for Air and Stream Improvement (NCASI).

Appendix: Statistics for evaluating model skill

Bias and several goodness-of-fit measures were the primary statistics used to evaluate model skill at reproducing climate variables and streamflow. The overall approach and certain definitions are taken from Legates and McCabe (1999), an excellent reference on goodness-of-fit measures.

Bias was defined as the ratio of predicted (simulated) mean to observed mean

$$bias = \frac{\bar{P}}{\bar{O}} \tag{1}$$

where

$\bar{P} =$ mean of the predictions
$\bar{O} =$ mean of the observations

The traditional R^2, or square of Pearson's product-moment correlation coefficient, describes the portion of total variance in the observed data that can be explained by the model, and ranges from 0.0 to 1.0:

$$R^2 = \left\{ \frac{\sum_{i=1}^{N} (O_i - \bar{O})(P_i - \bar{P})}{\left[\sum_{i=1}^{N} (O_i - \bar{O})\right]^{0.5} \left[\sum_{i=1}^{N} (P_i - \bar{P})\right]^{0.5}} \right\}^2 \tag{2}$$

where

$N =$ number of timesteps
$O_i =$ observed value at timestep i
$\bar{O} =$ mean of the observations
$P_i =$ the predicted value at timestep i
$\bar{P} =$ mean of the predictions.

There are two disadvantages of R^2 for describing model skill: 1) any linear relationship between the observations and the predictions, not necessarily a 1:1 relationship, results in a high value of R^2; 2) the squaring of terms gives too much weight to large values. In the case of streamflow, a high R^2 value may indicate good fit of peakflows, but may mask poor model skill during baseflow periods.

The Nash and Sutcliffe (1970) efficiency E is a tougher test than R^2 and casts the mean of the observations as a benchmark for the model:

$$E = 1.0 - \frac{\sum_{i=1}^{N} (O_i - P_i)^2}{\sum_{i=1}^{N} (O_i - \bar{O})^2}. \tag{3}$$

Values of E tend to be slightly less than R-squared in the case of streamflow.

Three first-degree goodness-of-fit measures from Legates and McCabe (1999) use absolute values of differences instead of squares. The first-degree efficiency is defined as

$$E_1 = 1.0 - \frac{\sum_{i=1}^{N} \mid O_i - P_i \mid}{\sum_{i=1}^{N} \mid O_i - \bar{O} \mid}. \tag{4}$$

E_1 is an improvement over E when evaluating model skill at low and moderate streamflow levels is important, but the grand mean is still the basis of comparison. A further discrimination can be gained by using a baseline mean involving some kind of seasonal or other categorical variation inherent in the data. Here, the the baseline mean was defined as the mean for each month of the year, where the mean is taken across all years in the simulation. Avoidance of squaring and use of baseline mean instead of the grand mean provides tougher, more revealing tests of model skill.

The baseline-adjusted, first-degree efficiency is

$$E_1' = 1.0 - \frac{\sum_{i=1}^{N} \mid O_i - P_i \mid}{\sum_{i=1}^{N} \mid O_i - \overline{O'} \mid} \tag{5}$$

where

$\overline{O'} =$ baseline mean of the observations, variable in time.

All of the above measures of efficiency have a possible range of $-\infty$ to 1.0. When efficiency=0, the model is no better or worse than the observed mean as a predictor. The closer the baseline mean is to the individual observations, the lower the efficiency is likely to be.

The baseline-adjusted modified index of agreement is

$$d_1' = 1.0 - \frac{\sum_{i=1}^{N} \mid O_i - P_i \mid}{\sum_{i=1}^{N} \left(\mid P_i - \overline{O'} \mid + \mid O_i - \overline{O'} \mid\right)}. \tag{6}$$

d_1' has the advantage of having the same range as the familiar R^2, 0 to 1.0.